

640 × 512 Pixel Long-Wavelength Infrared Narrowband, Multiband, and Broadband QWIP Focal Plane Arrays

Sarath D. Gunapala, Sumith V. Bandara, John K. Liu, Sir B. Rafol, and Jason M. Mumolo

Abstract—A 640 × 512 pixel, long-wavelength cutoff, narrowband ($\Delta\lambda/\lambda \sim 10\%$) quantum-well infrared photodetector (QWIP) focal plane array (FPA), a four-band QWIP FPA in the 4–15 μm spectral region, and a broadband ($\Delta\lambda/\lambda \sim 42\%$) QWIP FPA having a 15.4 μm cutoff have been demonstrated. In this paper, we discuss the electrical and optical characterization of these FPAs, and their performance. In addition, we discuss the development of a very sensitive (NEDT ~ 10.6 mK) 640 × 512 pixel thermal imaging camera having a 9 μm cutoff.

Index Terms—Broadband, focal plane array, infrared camera, long-wavelength infrared, mid-wavelength infrared, multiband, narrowband, quantum-well infrared photodetectors (QWIP).

I. INTRODUCTION

THE quantum-well infrared photodetectors (QWIPs) discussed in this article utilize the photoexcitation of electrons between the ground state and the first excited state in the conduction band quantum-well (QW) (see [1]–[3] for a detailed description on QWIPs). There has been much interest lately [1]–[6] in large format QWIP focal plane arrays (FPAs). In this paper we discuss the design, fabrication, and test results of 640 × 512 pixel narrowband, multiband, and broadband QWIP FPAs. These large format FPAs will be useful for many applications such as the *in-situ* and remote sensing of gas molecules, thermal imaging, global atmospheric temperature profiles monitoring, cloud characteristic measurements, astronomy, tracking and identification of missiles, etc.

II. NARROWBAND QWIP DEVICE

Each-period of the multiquantum-well (MQW) structure consists of a 45-Å well of GaAs (doped $n = 5 \times 10^{17} \text{ cm}^{-3}$) and a 500-Å barrier of $\text{Al}_{0.3}\text{Ga}_{0.7}\text{As}$. Stacking many identical QWs (typically 50) together increases photon absorption. Ground state electrons are provided in the detector by doping the GaAs well layers with Si. This photosensitive MQW structure is sandwiched between 0.5 μm GaAs top and bottom contact layers doped $n = 5 \times 10^{17} \text{ cm}^{-3}$, grown on a semi-insulating GaAs substrate by molecular beam epitaxy (MBE). Then a

Manuscript received April 10, 2003; revised July 18, 2003. This work was sponsored in part by the Breakthrough Sensors and Instrument Component Technology Thrust of the NASA Cross Enterprise Technology Development Program, and the NASA Earth Science Technology Office. The review of this paper was arranged by Editor P. Bhattacharya.

The authors are with the Jet Propulsion Laboratory, California Institute of Technology, Pasadena, CA 91109 USA (e-mail: Sarath.d.Gunapala@jpl.nasa.gov).

Digital Object Identifier 10.1109/TED.2003.818818

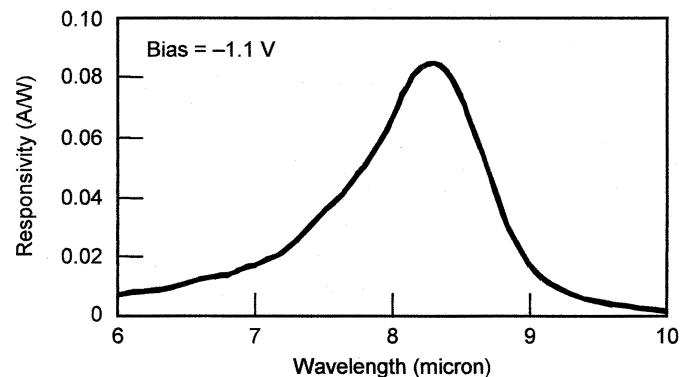


Fig. 1. Responsivity spectrum of a bound-to-quasibound LWIR QWIP test structure at temperature $T = 77$ K. The spectral response peak is at 8.5 μm and the long-wavelength cutoff is at 8.9 μm .

0.7- μm thick GaAs cap layer on top of a 300 Å $\text{Al}_{0.3}\text{Ga}_{0.7}\text{As}$ stop-etch layer was grown *in-situ* on top of the device structure to fabricate the light coupling optical cavity [1].

Test detectors with 200 μm diameter were fabricated and back illuminated through a 45° polished facet [1] for optical characterization and an experimentally measured responsivity spectrum is shown in Fig. 1. The responsivity of the detector peaks at 8.5 μm and the peak responsivity (R_P) of the detector is 83 mA/W at bias $V_B = -1.1$ V. The spectral width and the cutoff wavelength are $\Delta\lambda/\lambda = 10\%$ and $\lambda_c = 8.9 \mu\text{m}$, respectively.

The photoconductive gain g was experimentally determined using [1] $g = i_n^2/4eI_D\Delta f + 1/(2N)$, where Δf is the measurement bandwidth, N is the number of QWs, and i_n is the current noise, which was measured using a spectrum analyzer. Since the gain of QWIP is inversely proportional to the number of QWs N , the better comparison would be the well capture probability p_c , which is directly related to the gain [1] by $g = 1/(Np_c)$. The calculated well capture probability is 25% at low bias (i.e., $V_B = -1.1$ V). The peak detectivity is defined as $D_B^* = R_P\sqrt{A\Delta f}/i_n$, where R_P is the peak responsivity, A is the area of the detector and $A = 3.14 \times 10^{-4} \text{ cm}^2$. The measured peak detectivity at bias $V_B = -1.1$ V and temperature $T = 65$ K is $1 \times 10^{11} \text{ cm}\sqrt{\text{Hz}}/\text{W}$. These detectors show background limited performance (BLIP) at bias $V_B = -2$ V and temperature $T = 72$ K for a 300 K background with $f/2$ optics. It is worth noting that the photoconductive gain is not very important at BLIP operating conditions, and therefore, the detectivities scale solely as a function of absorption quantum efficiencies (i.e., net quantum efficiency/photoconductive gain) of the detectors.

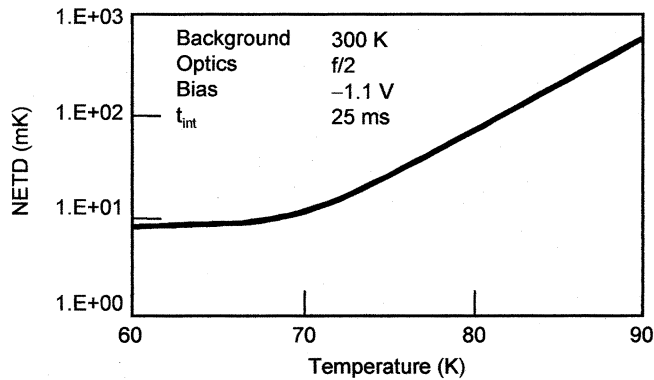


Fig. 2. Noise equivalent differential temperature NEDT estimated from test structure data as a function of temperature for bias voltage $V_B = -1.1$ V. The background temperature $T_B = 300$ K and the area of the pixel $A = (23 \mu\text{m})^2$.

III. 640×512 PIXEL NARROW-BAND FOCAL PLANE ARRAY

Several 640×512 pixel QWIP FPAs were fabricated as described elsewhere [1]. Twelve 640×512 pixel QWIP FPAs were processed on a 3-in GaAs wafer. The detector pixel pitch of the FPA is $25 \mu\text{m}$ and the actual pixel area is $23 \times 23 \mu\text{m}^2$. Indium bumps were evaporated on top of the detectors for hybridization with a silicon readout integrated circuit (ROIC). These QWIP FPAs were hybridized (via indium bump-bonding process) to a 640×512 pixel complementary metal-oxide semiconductor (CMOS) ROIC and biased at $V_B = -1.1$ V. At temperatures below 72 K, the signal-to-noise ratio of the system is limited by array nonuniformity, readout multiplexer (i.e., ROIC) noise, and photocurrent (photon flux) noise. At temperatures above 72 K, the temporal noise due to the dark current becomes the limitation. Charge injection efficiency into the ROIC was calculated as described in Bethea *et al.* [4]. An average charge injection efficiency of $\eta_{\text{inj}} = 90\%$ has been achieved at a frame rate of 30 Hz. This initial array gave excellent images with 99.92% of the pixels working (number of dead pixels ≈ 250), demonstrating the high yield of GaAs technology. The operability was defined as the percentage of pixels having noise equivalent differential temperature (NEDT) less than 100 mK at 300 K background (with $f/2$ cold-stop) and in this case operability happens to be equal to the pixel yield.

Fig. 2 shows the NEDT of the FPA estimated [1] from test structure data as a function of temperature for bias voltage $V_B = -1.1$ V. The background temperature $T_B = 300$ K, the area of the pixel $A = (23 \mu\text{m})^2$, the f number of the optical system is 2, and the frame rate is 30 Hz. Fig. 3 shows the measured NEDT histogram of the FPA at an operating temperature of $T = 65$ K, 16 ms integration time, bias $V_B = -1.1$ V for 300 K background with $f/2$ optics, and the mean value is 20 mK. The absorption quantum efficiency of the FPA was 10%, which also agrees closely with the single element test detector results.

IV. 640×512 PIXEL HAND-HELD CAMERA

A 640×512 QWIP FPA hybrid was integrated with a 330 mW integral Stirling closed-cycle cooler assembly and installed into an Indigo Phoenix™ camera-body to demonstrate a hand-held long-wavelength infrared (LWIR) camera. The

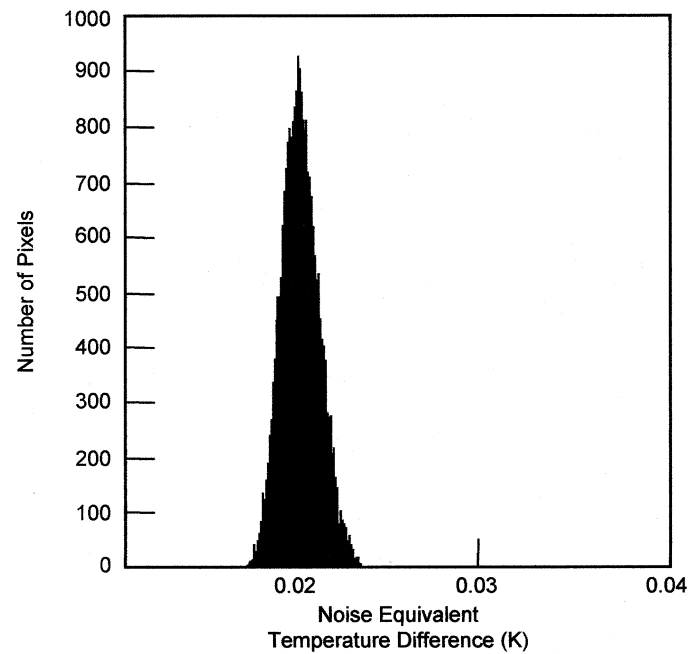


Fig. 3. NEDT histogram of the 327 680 pixels of the 640×512 array showing a high uniformity of the FPA. The uncorrected nonuniformity (= standard deviation/mean) of the FPA is only 5% including 1% nonuniformity of ROIC and 1.4% nonuniformity due to the cold-stop not being able to give the same field-of-view to all the pixels in the FPA. The nonuniformity was reduced to an impressive 0.02% after two-point correction. No $1/f$ noise was observed down to 10 mHz.

camera head consists of a 640×512 format LWIR QWIP array hybridized with Indigos ISC 9803 ROIC, a cold-stop, a Stirling cooler, preamplifiers, and analog-to-digital converters. The optical element of the camera is a 100-mm focal length germanium lens assembly, with a 9.2° field of view. It is designed to be transparent in the 7–14 μm wavelength range, to be compatible with the QWIPs 8.5 μm operation. The digital acquisition resolution of the camera is 14 bits, which determines the instantaneous dynamic range of the camera (i.e., 16,384). However, the dynamic range of QWIP is 85 dB.

The measured mean NEDT of the QWIP camera system is 20 mK at an operating temperature of $T = 65$ K and bias $V_B = -1.1$ V for a 300 K background with germanium $f/2$ optics. The uncorrected photocurrent nonuniformity (which includes a 1% nonuniformity of the ROIC and a 1.4% nonuniformity due to the cold-stop in front of the FPA not yielding the same field of view to all the pixels) of the 327 680 pixels of the 640×512 FPA is about 5% (= sigma/mean). The nonuniformity after a two-point (17° and 27°C correction improves to an impressive 0.02%. Fig. 4 shows four frames of video images taken with this large format LWIR camera at 6 h time intervals within a day.

The FPA performance data reported in this paper was taken with the first LWIR Phoenix™ camera. Estimates based on the single pixel data show that these FPAs should be able to provide 7 mK NEDT with a 30 ms integration time, which can be achieved at $V_B = 1.1$ V bias. As shown in Fig. 3, the measured NEDT of the LWIR QWIP Phoenix™ camera is 20 mK with a 16 ms integration time. The noise of the camera system can be written as, $N_{\text{SYS}}^2 = n_{\text{Detector}}^2 + n_{\text{ADC}}^2 + n_{\text{MUX}}^2$, where n_{Detector}



Fig. 4. Four frames of video images taken with the $9\ \mu\text{m}$ cutoff 640×512 pixel QWIP Phoenix™ camera. These four images were taken at 6 h time intervals during a single day. Top left (6 am), top right (noon), lower left (6 pm), and lower right (midnight).

is the noise of the FPA, n_{ADC} is the noise of the analog-to-digital converter, and n_{MUX} is the noise of the silicon ROIC. The experimentally measured N_{SYS} is 2 units, and the n_{ADC} and n_{MUX} are 0.8 and 1 unit, respectively. This yields 1.5 noise units for n_{Detector} . Thus, the NEDT of the FPA is 15 mK at 300 K background with $f/2$ optics and 16 ms integration time. This agrees reasonably well with our estimated value of 10 mK based on test detector data (see Fig. 2). Therefore, these FPAs should be able to achieve 10.6 mK NEDT at the same operating conditions with 32 ms integration time.

V. VERTICALLY INTEGRATED FOUR-BAND QWIP DEVICE

This four-band vertically integrated device structure was achieved by the growth of multistack QWIP structures separated by heavily doped n^+ contact layers, on a semi-insulating GaAs substrate. Device parameters of each QWIP stack were designed to respond in different wavelength bands. Fig. 5 shows the schematic device structure of a four-band QWIP FPA. A typical QWIP stack consists of a MQW structure of GaAs QWs

separated by thick (i.e., 500–600 Å) $\text{Al}_x\text{Ga}_{1-x}\text{As}$ barriers. The actual device structure consists of a 15-period stack of 4–6 μm QWIP structure, a 25-period stack of 8.5–10 μm QWIP structure, a 25-period stack of 10–12 μm QWIP structure and a 30-period stack of 13–15 μm QWIP structure. Each photosensitive MQW stack was separated by a heavily doped n^+ (thickness 0.2 to 0.8 μm) intermediate GaAs contact layer. Since the dark current of this device structure is dominated by the longest wavelength portion of the device structure, the very long-wavelength infrared (VLWIR) QWIP structure has been designed to have a bound-to-quasibound intersubband absorption peak at 14.0 μm . Other QWIP device structures have been designed to have a bound-to-continuum intersubband absorption process because the photo current and dark current of these devices are relatively small compared to the VLWIR device. This whole four-band QWIP device structure was then sandwiched between 0.5 μm GaAs top and bottom contact layers doped with $n = 5 \times 10^{17}\ \text{cm}^{-3}$ and was grown on a semi-insulating GaAs substrate by MBE.

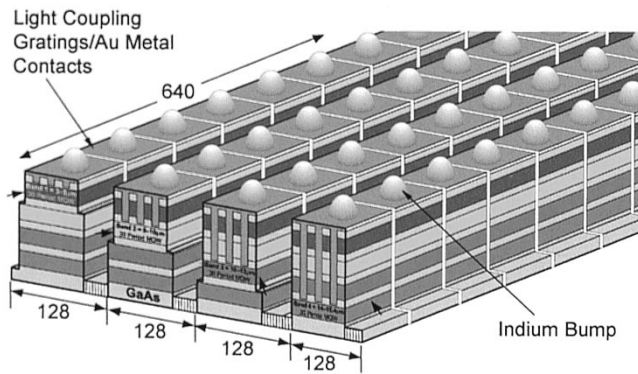


Fig. 5. Layer diagram of the four-band QWIP device structure and the deep groove two-dimensional-periodic grating structure. Each pixel represent a 640×128 pixel area of the four-band focal plane array.

VI. A 640×512 PIXEL FOUR-BAND SPATIALLY SEPARATED FOCAL PLANE ARRAY

In this section, we discuss the demonstration of the first 640×512 pixel monolithic spatially separated four-band QWIP FPA. The unique feature of this spatially separated four-band FPA is that the four infrared bands are independently and simultaneously readable on a single imaging array. The multiband FPAs based on narrowband QWIP detector structures have the advantage over other broadband detectors such as HgCdTe in that the spectral responses of QWIP are relatively narrow so that a detector designed for a specific spectral band only detects radiation in that band with little or no spectral crosstalk [5]. Thus, pixel co-located multiband QWIP FPAs can operate in simultaneous read mode compared to the alternate frame read mode of multiband FPAs based on other detector technologies [5]. These advantages lead to a reduction in instrument size, weight, mechanical complexity, optical complexity and power requirements since no moving parts are needed. Furthermore, a single optical train can be employed, and the whole focal plane can operate at a single temperature.

The individual pixels of the four-color FPA were defined by photolithographic processing techniques (masking, dry etching, chemical etching, metal deposition, etc.). Four separate detector bands were defined by a deep trench etch process and the unwanted spectral bands were eliminated by a detector short-circuiting process. The unwanted top detectors were electrically shorted by gold-coated reflective two-dimensional etched gratings as shown in the Fig. 5. In addition to shorting, these gratings serve as light couplers for active QWIP stack in each detector pixel [6]. Design and optimization of these two-dimensional gratings to maximize QWIP light coupling are extensively discussed elsewhere [1]. The unwanted bottom QWIP stacks were electrically shorted at the end of each detector pixel row.

Typically, quarter-wavelength deep ($h = \lambda_p/4n_{\text{GaAs}}$) grating grooves are used for efficient light coupling in single-band QWIP FPAs. However, in this case, the height of the quarter-wavelength deep grating grooves is not deep enough to short circuit the top three MQW QWIP stacks (e.g.: three top QWIP stacks on $13\text{--}15\ \mu\text{m}$ QWIP in Fig. 5). Thus, three-quarter-wavelength groove depth two-dimensional gratings ($h = 3\lambda_p/4n_{\text{GaAs}}$) were used to short the top unwanted detectors over the $10\text{--}12$ and $13\text{--}15\ \mu\text{m}$ bands. This technique

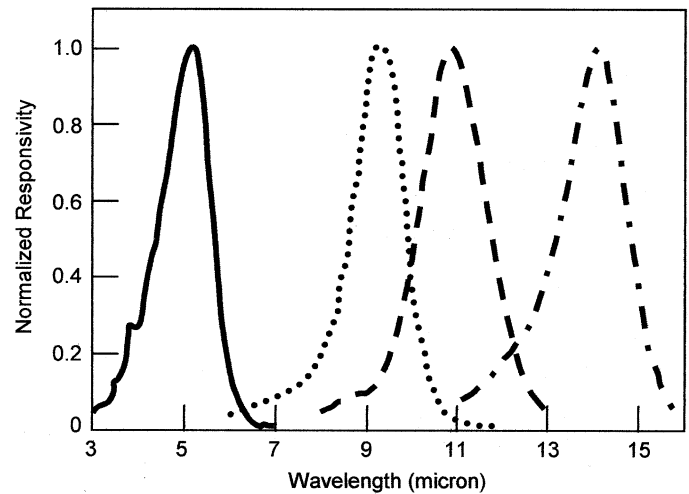


Fig. 6. Normalized spectral response of the four-band QWIP FPA.

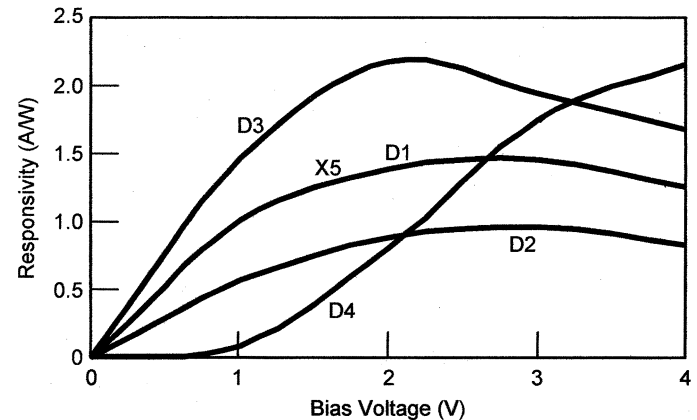


Fig. 7. Bias dependent peak responsivities of the detectors in four-band QWIP FPA. The peak response wavelength for detectors D1, D2, D3, and D4 are $\lambda_p = 5\ \mu\text{m}$, $\lambda_p = 9.1\ \mu\text{m}$, $\lambda_p = 11\ \mu\text{m}$, and $\lambda_p = 14.2\ \mu\text{m}$, respectively. The responsivity curve for detector D1 is multiplied by a factor of 5 to fit to the scale.

optimized the light coupling to each QWIP stack at corresponding bands while keeping the pixel (or mesa) height at the same level which is essential for the indium bump-bonding process used for detector array and readout multiplexer hybridization. Fig. 6 shows the normalized spectral responsivities of all four spectral bands of this four-band FPA. Spectral band widths of the four detectors from shorter wavelength to longer wavelength in increasing order are $\Delta\lambda/\lambda_p \sim 26\%$, 15% , 17% , and 11% , respectively. Fig. 7 shows the measured absolute responsivity at the peak wavelength for all four detectors. As expected, the narrower bandwidth and the flat responsivity near zero bias voltage indicate the bound-to-quasibound nature transition in the VLWIR detector [1]. Detectors in the $8.5\text{--}10$ and $10\text{--}12\ \mu\text{m}$ spectral-bands show a slightly broader spectral bandwidth, with increasing responsivity right at the beginning of the bias voltage, confirming the bound-to-continuum design [1]. The typical spectral width of a MWIR QWIP is about $0.5\ \mu\text{m}$. The MWIR detector in this FPA is specifically designed to cover a $4\text{--}6\ \mu\text{m}$ wavelength range with $\Delta\lambda/\lambda_p \sim 26\%$ broader responsivity by utilizing three coupled QWs in each-period of the MQW stack [7]. Also, the shorter wavelength response

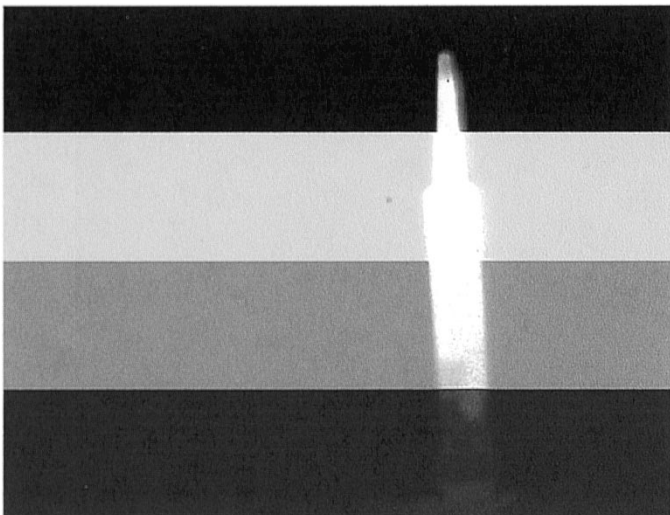


Fig. 8. One frame of video image taken with the 4–15 mm cutoff four-band 640 × 512 pixel QWIP camera. The image is barely visible in the 13–15 μm spectral band due to the poor optical transmission of the anti-reflection layer coated germanium lens.

in this detector is achieved by using deeper $\text{In}_{0.33}\text{Ga}_{0.67}\text{As}$ QWs with lattice mismatched $\text{Al}_{0.3}\text{Ga}_{0.7}\text{As}$ barriers [7]. A high Al ratio is less desirable in these detectors because of the high defect density and the near crossing of the Γ and X valleys [1]. Also, the utilization of the coupled QWs within the MQW structure creates unbiased energy subbands where photoexcited electrons can be easily relaxed before reaching the collector contact. These reasons could result in a very low optical responsivity in MWIR detector as seen in Fig. 7.

A few QWIP FPAs were chosen and hybridized to a 640 × 512 pixel silicon CMOS ROIC and biased at $V_B = -1.5$ V. At temperatures below 100 K, the signal-to-noise ratio of the 4–6 μm spectral band is limited by array nonuniformity, multiplexer readout noise, and photo current (photon flux) noise. At temperatures above 40 K, temporal noise due to the 13–15 μm QWIPs higher dark current becomes the limitation. The 8.5–10 and 10–12 μm spectral bands have shown BLIP performance at temperatures between 45 and 83 K. This initial array gave excellent images with 99.9% operability (number of dead pixels ≈ 250).

A 640 × 512 pixel four-band QWIP FPA hybrid was mounted onto a 84-pin lead-less chip carrier and installed into a laboratory dewar which is cooled by liquid helium to demonstrate a four-band simultaneous imaging camera. The FPA was cooled to 45 K and the temperature was stabilized by a temperature controller and regulating the pressure of gaseous helium. The optical assembly of the FPA test setup consists a 100-mm focal length antireflection coated germanium lens, which gives a 9.2° field of view. A SEIR image processing station was used to obtain clock signals for the readout multiplexer and to perform digital data acquisition and nonuniformity corrections. The digital data acquisition resolution of the camera is 14 bits, which determines the instantaneous dynamic range of the camera (i.e., 16,384). Video images were taken at a frame rate of 30 Hz at temperatures as high as $T = 45$ K, using a ROIC capacitor having a charge capacity of 11×10^6 electrons. Fig. 8 shows one frame of a video image taken with the four-band 640 × 512

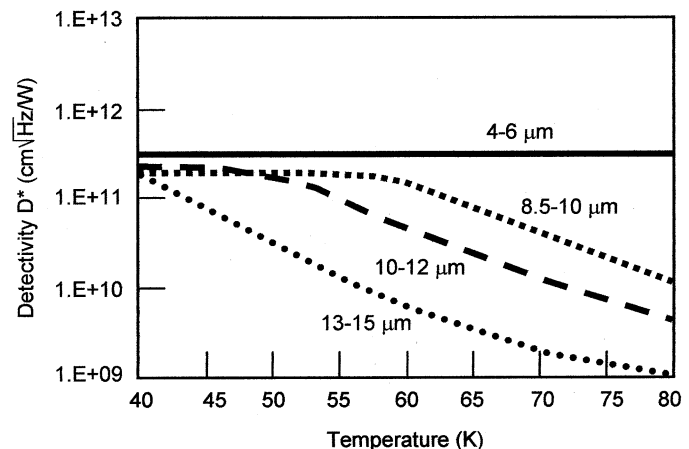


Fig. 9. Detectivities of each spectral-band of the four-band QWIP FPA as a function of temperature. Detectivities were estimated using the single pixel test detector data taken at $V_B = -1.5$ V and 300 K background with $f/5$ optics.

pixel QWIP FPA. It is noticeable that the object in the 13–15 μm band is not very clear due to the reduced optical transmission of the germanium lens beyond 14 μm .

Fig. 9 shows the peak detectivities of all four spectral bands as a function of operating temperature. Based on single element test detector data, the 4–6, 8.5–10, 10–12, and 13–15 μm spectral bands show BLIP at temperatures 40, 50, 60, and 100 K, respectively, for a 300 K background with a $f/5$ cold stop. As expected (due to BLIP), the estimated and experimentally obtained NEDT values of all spectral-bands do not change significantly below their BLIP temperatures. The experimentally measured NEDT of 4–6, 8.5–10, 10–12, and 13–15 μm detectors at 40 K are 21, 45, 14, and 44 mK, respectively (see Fig. 10). The experimentally observed NEDT values of 4–6 and 10–12 μm spectral bands agree reasonably well with the estimated NEDT values based on the single element test detector data. On the other hand, the NEDT values obtained for 8.5–10 and 13–15 μm spectral bands are almost a factor of two higher than the estimates based on single element test detector data. This decrease in performance attribute to the processing related nonuniformity. This is clearly evident from the wider NEDT histograms of the 8.5–10 and 13–15 μm spectral bands. Scanning electron micrographs show that this nonuniformity was mostly associated with the top detector short-circuiting via deep groove grating structure.

VII. BROADBAND QWIP DEVICE

The broadband QWIP device structure was designed by repeating a unit of several QWs with slightly different parameters such as well width and barrier height [9]. The positions of ground and excited states of the QW are determined by the QW width (L_w) and the barrier height, i.e., the Al mole fraction (x) of the barrier. Since each single set of parameters for a bound-to-quasibound QW [1] corresponds to a spectral band pass of about 1.5 μm , three different sets of values are sufficient to cover a 10–16 μm spectral region. The MQW structure consists of many periods of these three QW units separated by thick barriers [8].

The device structure reported here involved 33 repeated layers of GaAs three-QW units separated by $L_B \sim 575$ Å-thick $\text{Al}_x\text{Ga}_{1-x}\text{As}$ barriers. The well thickness of the QWs of the

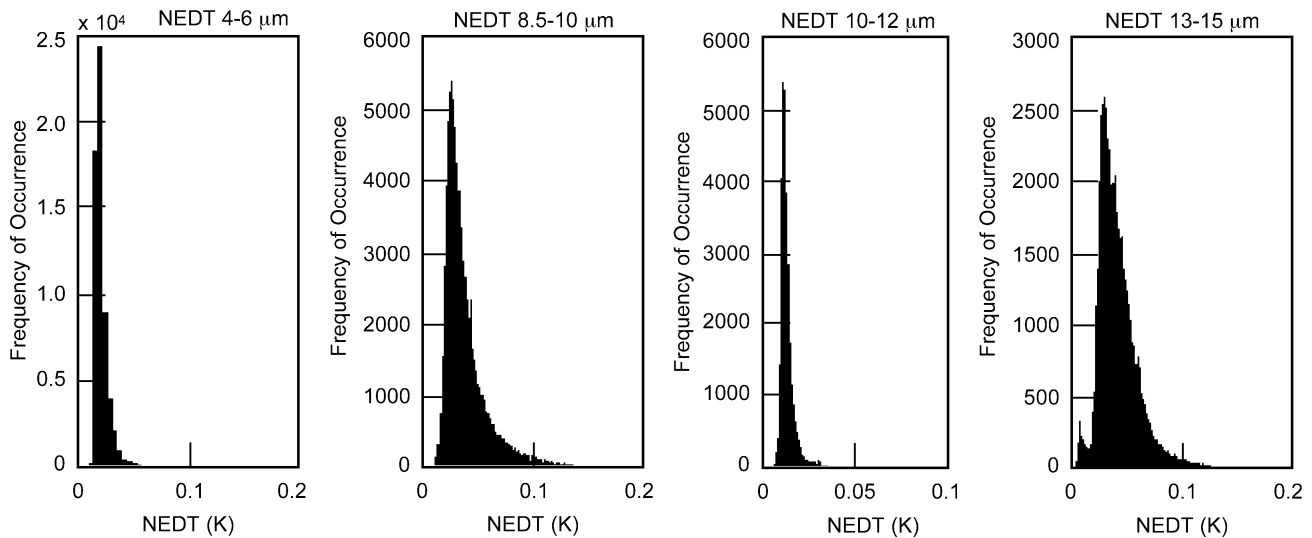


Fig. 10. NEDT histogram of the 640×512 pixel spatially separated four-band focal plane showing a high uniformity of the FPA. Each spectral band of the FPA consisted of 640×128 pixels. The experimentally measured NEDT of 4–6, 8.5–10, 10–12, and 13–15 μm detectors at 40 K are 21, 45, 14, and 44 mK, respectively.

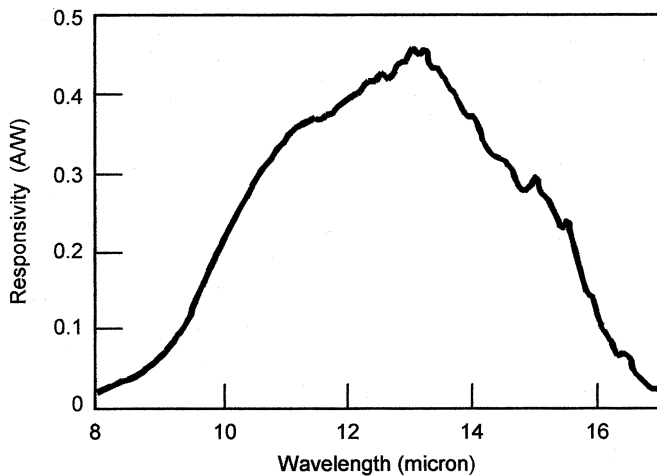


Fig. 11. Responsivity spectrum of a broadband QWIP test structure at temperature $T = 55$ K. The spectral response peak is at $13.5 \mu\text{m}$ and the long-wavelength cutoff is at $15.4 \mu\text{m}$.

three-QW units are designed to respond at peak wavelengths around 13, 14, and $15 \mu\text{m}$, respectively. These wells are separated by $L_u \sim 75 \text{ \AA}$ thick $\text{Al}_x\text{Ga}_{1-x}\text{As}$ barriers. The Al mole fraction (x) of barriers throughout the structure was chosen such that the $\lambda_p = 13 \mu\text{m}$ QW operates under bound-to-quasibound conditions. The excited state energy level broadening has been further enhanced due to the overlap of the wavefunctions associated with excited states of QWs separated by thin barriers [8]. Energy band calculations based on a two band model show excited state energy levels spreading about 28 meV.

This device structure was grown on a semi-insulating 3-in GaAs substrate by using MBE growth technique. Test detectors were fabricated as described elsewhere for electrical and optical characterization of the detector material. In Fig. 11, the responsivity curve at $V_B = -2.5$ V bias voltage shows broadening of the spectral response up to $\Delta\lambda \sim 5.5 \mu\text{m}$, (i.e., the full width at half-maximum from 10.5 – $16 \mu\text{m}$). This broadening $\Delta\lambda/\lambda_p \sim 42\%$ is about a 400% increase compared to a typical bound-to-quasibound QWIP. The responsivity of the detector

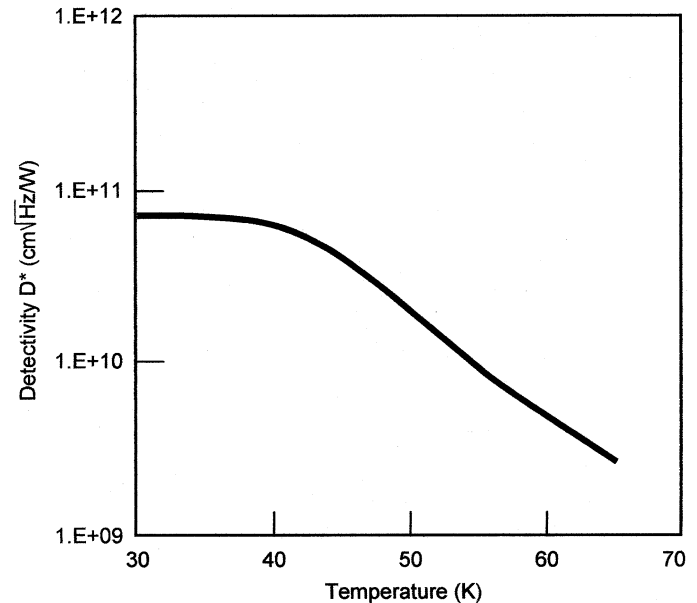


Fig. 12. Detectivity as a function of temperatures at bias voltage $V_B = -2.5$ V.

peaks at $13.5 \mu\text{m}$ and the peak responsivity (R_p) of the detector is 250 mA/W at bias $V_B = -2.5$ V. The peak absorption quantum efficiency was 11% at bias $V_B = -2.5$ V for a 45° double pass.

The dark current noise i_n of the device was measured using a spectrum analyzer at $T = 55$ K as a function of bias voltage. The photoconductive gain g can now be obtained using the generation-recombination noise calculated based on the standard noise expression given [1]. Using experimental measurements of noise and responsivity, one can now calculate specific detectivity D^* [1]. The calculated D^* value for the present device ($\lambda = 15.4 \mu\text{m}$) at $T = 55$ K and $V_B = 2.5$ V is $3 \times 10^{10} \text{ cm}^2\sqrt{\text{Hz}}/\text{W}$. Even with broader response, this D^* is comparable to previously reported D^* of QWIPs with narrow spectral response. Fig. 12 shows the detectivity D^* as a function of the operating temperature of the device.

VIII. A 640 × 512 PIXEL BROADBAND QWIP FOCAL PLANE ARRAY

Though two-dimensional grating is an efficient light coupler, it is not suitable for broadband QWIPs due to its inherent narrowband light coupling efficiency. Thus, we have implemented a wide-ranged random reflector for coupling normal incident radiation into broadband QWIPs [1]. The broadband 640 × 512 pixel QWIP FPAs were then fabricated using standard FPA fabrication techniques [1]. The pixel pitch of the FPA is 25 μm and the actual pixel size is 23 × 23 μm^2 . These broadband QWIP FPAs were hybridized via an indium bump-bonding process to a 640 × 512 pixel silicon CMOS ROIC and biased at $V_B = -2.5$ V. At temperatures below 40 K, the signal-to-noise ratio of the system is limited by array nonuniformity, multiplexer readout noise, and photo current (photon flux) noise. At temperatures above 40 K, temporal noise due to the dark current becomes the limitation. Due to the QWIPs high impedance, a charge injection coupling efficiency into the integration capacitor of the multiplexer $\eta_{\text{inj}} = 99.5\%$ was achieved at a frame rate of 30 Hz. This initial array gave very good images with 99.9% operability.

The mean value of the experimentally measured NEDT histogram of the FPA at an operating temperature of $T = 40$ K, bias $V_B = -2.5$ V at 300 K background with $f/2$ optics is 55 mK. This agrees reasonably well with our estimated value of 25 mK based on test structure data. The read noise of the multiplexer is 500 electrons. The factor of two shortfall of NEDT is mostly attributed to a decrease in bias voltage across the detectors during charge accumulation (common in many direct-injection type readout multiplexers) and read noise of the readout multiplexer. The experimentally measured peak quantum efficiency of the FPA was 9.5%, which agrees well with the 11% absorption quantum efficiency estimated from the single element detector data.

In summary, we have demonstrated the first 640 × 512 pixel spatially separated monolithic four-band detector array and the first 640 × 512 pixel broadband FPA. We also have discussed the demonstration of a very sensitive 640 × 512 pixel portable LWIR imaging camera. All QWIP FPAs were back-illuminated through the flat thinned substrate membrane (thickness ≈ 1000 Å). This thinned GaAs FPA membrane has completely eliminated the thermal mismatch between the silicon CMOS ROIC and the GaAs based QWIP FPA, and has completely eliminated the pixel-to-pixel optical cross-talk of the FPA. These FPAs can be used in many ground based and space borne applications that require long-wavelength, large, uniform, reproducible, and low $1/f$ noise [1] narrowband, multiband, and broadband LWIR FPAs.

ACKNOWLEDGMENT

The authors would like to express their gratitude to C. P. Bankston, M. Bothwell, T. Krabach, and P. Grunthner of the Jet Propulsion Laboratory, P. D. LeVan of the Air Force Research Laboratory, and M. Z. Tidrow of the Missile Defense Agency for the encouragement and support during the development of novel QWIP FPAs at the Jet Propulsion Laboratory for various applications. Also, the authors would like to give their

special thanks to F. Reininger of the Jet Propulsion Laboratory, J. Woolaway, C. A. Shott, and R. Jones of the Indigo System Corporation, M. Jhabvala of the NASA Goddard Space Flight Center, and K. K. Choi of Army Research Laboratory for stimulating technical discussions.

REFERENCES

- [1] S. D. Gunapala and S. V. Bandara, "quantum-well infrared photodetector (QWIP) focal plane arrays," in *Semiconductor Semimetals*, H. C. Liu and F. Capasso, Eds. San Diego, CA: Academic, 2000, vol. 62, pp. 197–282.
- [2] B. F. Levine, "Quantum-well infrared photo-detectors," *J. Appl. Phys.*, vol. 74, pp. R1–R81, 1993.
- [3] H. C. Liu, "quantum-well infrared photodetector physics and novel devices," in *Semiconductor Semimetals*, H. C. Liu and F. Capasso, Eds. San Diego, CA: Academic, vol. 62, pp. 126–196.
- [4] C. G. Bethea, B. F. Levine, M. T. Asom, R. E. Leibenguth, J. W. Stayt, K. G. Glogovsky, R. A. Morgan, J. Blackwell, and W. Parish, "long-wavelength infrared 128 × 128 $\text{Al}_x\text{Ga}_{1-x}\text{As}/\text{GaAs}$ quantum-well infrared camera and imaging system," *IEEE Trans. Electron Devices*, vol. 40, pp. 1957–1963, Nov. 1993.
- [5] A. C. Goldberg, S. W. Kennerly, J. W. Little, H. K. Pollehn, T. A. Shafer, C. L. Mears, H. F. Schaake, M. Winn, M. Taylor, and P. N. Uppal, "Comparison of HgCdTe and QWIP dual-band focal plane arrays," *Opt. Eng.*, vol. 42, pp. 30–46, 2003.
- [6] S. D. Gunapala, S. V. Bandara, A. Singh, J. K. Liu, S. B. Rafol, E. M. Luong, J. M. Mumolo, N. Q. Tran, D. Z.-Y. Ting, J. D. Vincent, C. A. Shott, J. Long, and P. D. LeVan, "640 × 486 long-wavelength two-color GaAs/AlGaAs quantum-well infrared photodetector (QWIP) focal plane array camera," *IEEE Trans. Electron Devices*, vol. 47, pp. 963–971, May 2000.
- [7] K. K. Choi, S. V. Bandara, S. D. Gunapala, W. K. Liu, and J. M. Fastenau, "Detection wavelength of InGaAs/AlGaAs quantum-wells and superlattices," *J. Appl. Phys.*, vol. 91, pp. 551–564, 2002.
- [8] S. V. Bandara, S. D. Gunapala, J. K. Liu, E. M. Luong, J. M. Mumolo, W. Hong, D. K. Sengupta, and M. J. McKelvey, "10–16 μm broadband quantum-well infrared photodetector," *Appl. Phys. Lett.*, vol. 72, pp. 2427–2429, 1998.



Sarath D. Gunapala received the Ph.D. degree in physics from the University of Pittsburgh, Pittsburgh, PA, in 1986.

He studied infrared properties of III–V compound semiconductor hetero-structures and the development of quantum-well infrared photodetectors (QWIPs) for infrared imaging at AT&T Bell Laboratories, Murray Hill, NJ, from 1986 to 1992. He joined NASA's Jet Propulsion Laboratory, California Institute of Technology, Pasadena, in 1992 as a Senior Research Scientist and a Principal Engineer

where he also leads the Infrared Focal Planes and Photonics Technology Research Group there. He holds several patents, and has authored over 150 publications, including several book chapters on QWIP imaging focal plane arrays.



Sumith V. Bandara received the Ph.D. degree in physics from the University of Pittsburgh, Pittsburgh, PA, in 1989

He is a Senior Member of Technical Staff in the Infrared Focal Plane and Photonic Technology Group, Jet Propulsion Laboratory (JPL), Pasadena, CA. He has over ten years of experience in semiconductor devices including quantum-well infrared photodetector research. Prior to joining the JPL, he worked at the Bell Laboratories, Murray Hill, NJ, and at the University of Pittsburgh where his work involved new semiconductor device design, theoretical modeling, fabrication, optical coupling, and performance analysis. He has authored and co-authored over 80 technical publications, including extensive reviews on QWIPs.



John K. Liu received the B.S. degree in engineering science and bioengineering from the University of California at San Diego, La Jolla, in 1984, and the M.S.E.E. degree from California State University, Los Angeles, in 1986.

From 1985 to 1989 he worked at NASA's Jet Propulsion Laboratory (JPL), California Institute of Technology, Pasadena, on solar cell and III-V MBE growth. From 1989 to 1991 he worked at TRW, Redondo Beach, CA, on III-V thin film growth using MBE for MMIC applications. Since 1991 he has

been working on the development of QWIP IR camera at the JPL. His current research interest is on QWIP FPA fabrications and characterizations.



Jason M. Mumolo received the B.S. degree in electrical engineering from the Polytechnic University of California, Pomona, in 2001.

He joined NASA's Jet Propulsion Laboratory, California Institute of Technology, Pasadena, in 1997 as an undergraduate, part-time student. Upon graduating, he joined the Infrared Focal Planes and Photonics Technology Group fulltime as a Process Engineer. His current work and research interest is in the development and fabrication of QWIP devices and focal plane arrays for camera systems.



Sir B. Rafol received the B.E.E.T. degree from DeVry Institute of Technology, Chicago, IL, in 1976, the M.A. degree in physics from Kent State University, Kent, OH, in 1982, and the Ph.D. degree in physics from University of Illinois, Chicago, in 1991.

He joined USRobotics, Mount Prospect, IL, in 1995 and Rockwell, Woods Dale, IL, in 1997, where he worked on telecommunication systems. In 1998, he joined NASA's Jet Propulsion Laboratory, California Institute of Technology, Pasadena, where

he has been working on characterization of QWIP focal plane array, detector development, and system testing. His research interest is on transport properties of low-dimensional quantum systems and quantum detectors.